American Mineralogist, Volume 80, pages 757–764, 1995

# The oxygen isotope anatomy of a slowly cooled metamorphic rock

JOHN M. EILER,* JOHN W. VALLEY
Department of Geology and Geophysics, University of Wisconsin, Madison, Wisconsin 53706, U.S.A.
COLIN M. GRAHAM
Department of Geology and Geophysics, University of Edinburgh, Edinburgh, Scotland, U.K.
LUKAS P. BAUMGARTNER
Department of Geology and Geophysics, University of Wisconsin, Madison, Wisconsin 53706, U.S.A.

## ABSTRACT

The distribution of O isotope ratios in a slowly cooled metamorphic rock is investigated by a combination of ion microprobe and laser probe techniques. The sample has unusually simple geometry: centimeter-size domains of feldspar and garnet separated by a one-millimeter to one-centimeter thick layer of millimeter-size magnetite grains. Isotopic zonation at two different scales is documented. A sharp decrease in $\delta^{18}O$ in the outer 10–100 $\mu$m of individual magnetite grains is in agreement with modeling of isotopic reequilibration during cooling by interdiffusion between feldspar and magnetite. The presence of this zonation in the outer portions of magnetite grains that are adjacent to garnet indicates extensive transport along grain boundaries during diffusive exchange. Millimeter-scale zonation in the polygranular layer of magnetite is caused by the interaction of volume diffusion and grain boundary transport, the effects of which depend upon local textures. Grain boundaries enhance bulk diffusion in polygranular aggregates and allow exchange between nontouching grains. The results document a complex textural control to millimeter-scale O isotope zonation and geothermometry in slowly cooled rocks and document the importance of fast grain boundary transport in controlling diffusive exchange.

## INTRODUCTION AND SAMPLE DESCRIPTION

Diffusion is recognized as one of the principal kinetic pathways by which chemical and isotopic redistribution occurs in rocks. An extensive body of experiments and a growing number of field-based studies have demonstrated the importance of volume diffusion in the transport of the stable isotopes within many of the common rock-forming minerals (Freer, 1981; Valley and Graham, 1991; Brady, 1995; Eiler et al., 1995). However, applying our knowledge of volume diffusion to transport in rocks also requires an understanding of the role of grain boundaries and intergranular fluids in diffusion-controlled exchange. The evidence for grain boundary transport rates in rocks is limited compared with that for volume diffusion, and models of diffusional exchange have previously described end-member cases of either negligible or extremely fast grain boundary transport (e.g., Lasaga, 1983, vs. Eiler et al., 1992). This study applies the most recent advances in stable isotope analysis to test these competing hypotheses.

Ion microprobe analysis of $\delta^{18}O$ in 10 $\mu$m domains of electrically conducting minerals such as iron titanium oxides with a precision of $\pm 1.0‰$ is now routine, whereas the laser probe can achieve 0.1‰ precision on larger domains (~500 $\mu$m) of most silicates and oxides. Previous studies using only one of these techniques have demonstrated their usefulness in studying inter- and intracrystalline diffusion, mineral growth, and recrystallization (Valley and Graham, 1991, 1993; Hervig, 1992; Sharp, 1991; Elsenheimer and Valley, 1993; Kohn et al., 1993). This study combines both techniques in the analysis of a slowly cooled regional metamorphic rock. The results document the relationship between micrometer- and millimeter-scale processes in producing the isotope anatomy of rocks.

The sample investigated in this study (49-37-14B) is from the Benson Mines in the Adirondack Mountains, New York, U.S.A. The sample was collected from a zone of aluminous magnetite ore near the foot-wall of the deposit. It contains magnetite, garnet, and potassium feldspar, as well as lesser amounts of apatite, pyrrhotite, and biotite (not all of these are found in mutual textural equilibrium). Additional trace phases include pyrite, corundum, spinel (hercynite-gahnite), and dumortierite. Hematite is present as a trace alteration phase of magnetite but was scarce enough to be avoided in isotopic analysis. The main constituent minerals are concentrated into polygranular domains dominated by either magnetite, garnet, or feldspar. These domains are typically 5–20 mm

* Present address: Division of Geological and Planetary Sciences, California Institute of Technology, Pasadena, California 91125, U.S.A.

0003–004X/95/0708–0757$02.00

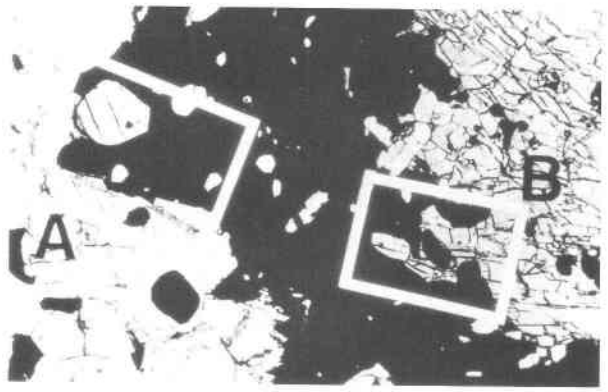


Fig. 1. Transmitted light photomicrograph of sample 49-37-14B. Black grains concentrated in the center are magnetite, bounded on the left by alkali feldspar and on the right by garnet. Areas A and B refer to regions where ion microprobe analyses were concentrated. The field of view is 18 mm wide.

in any given dimension. Individual grains are 0.5–3.0 mm in size. Magnetite contains exsolution lamellae of hercynite, which are ubiquitous but present in only trace amounts. Magnetite is near end-member $Fe_3O_4$ by electron microprobe analysis, with ca. 1.0 mol% hercynite. Previous studies of O isotope zonation in magnetite have identified alteration features that facilitate fluid-hosted alteration and low-temperature isotope exchange (Valley and Graham, 1993; Eiler et al., 1995). Acid etching (full strength, cold HCl) and inspection of ion microprobe pits after analysis indicate that this sample is free of such features. A 1.5 × 2 × 5 cm chip was used to prepare two facing thick sections. One (Fig. 1) was polished using a lead-lap for ion microprobe analysis in order to ensure the flat grain-to-grain contacts needed for analysis within 25 $\mu$m of grain boundaries, the other was used to prepare laser probe samples using the thin-saw technique (Elsenheimer and Valley, 1993; Kohn et al., 1993).

The Fe-rich siliciclastic sediments that made up the protolith of this deposit underwent granulite facies metamorphism (750–760 °C, 700–800 MPa: Marcotty, 1985; Bohlen et al., 1985) during the Grenville orogeny (1070–1050 Ma: McLelland et al., 1988; McLelland and Chiarenzelli, 1991). Some rocks at Benson Mines preserve metamorphic hematite, indicating that $f_{O_2}$ was appreciably higher than that found in surrounding rocks, which were near the quartz + fayalite + magnetite buffer (Marcotty, 1985). This indicates that fluid-flow or meter-scale equilibration through a fluid phase during metamorphism was limited or absent. Metamorphism was followed by cooling at 1–3 °C/m.y. (Mezger et al., 1990). Slow cooling favored diffusional redistribution of isotopes during retrogression.

## Results

### Ion microprobe analyses of magnetite

Ion microprobe analyses of O isotope ratios in magnetite were made using a Cameca IMS-4f, following the technique of Valley and Graham (1991). Standardization was made relative to LP204-1 magnetite, which has isotopic and chemical compositions close to those of the unknown. Fifty-five analyses of the sample were made during three sessions, with a total of 38 additional analyses of the standard (Table 1). The internal precision of each analysis is ±1.0‰ (1$\sigma$) based on counting statistics and the total number of secondary $^{18}O$ ions detected (~$10^6$). The standard deviation about the mean, average drift correction, and average instrumental fractionation for the standards averaged ±0.84‰ (1$\sigma$), 0.15‰ (per analysis), and −15.4‰ (~1‰ per atomic mass unit), respectively. These values are comparable to those found in previous studies (Valley and Graham, 1991; Eiler et al., 1995). Comparisons between ion microprobe and laser probe data from the same part of the sample analyzed in this study confirm the accuracy of these data; standardization introduces no significant uncertainties beyond the internal precision of each analysis.

Figure 1 is a transmitted light photomicrograph of the thin section prepared for ion microprobe analyses. Fifty analyses were concentrated into two regions outlined in Figure 1: region A, the margin of a magnetite-rich zone adjacent to feldspar (40 analyses), and region B, the margin of this magnetite-rich zone adjacent to garnet (ten analyses). Additional analyses were made in the interior of the magnetite-rich zone between these two areas to complete a traverse from the feldspar-magnetite contact to the magnetite-garnet contact.

The data show a difference in $\delta^{18}O$ from over 2‰ in the interior of the magnetite zone towards lower values at its margins (Fig. 2A–2C). This is most pronounced within 100 $\mu$m of the feldspar-magnetite contact, where seven out of ten analyses are <1‰, and none is >2‰. In contrast, two-thirds of the analyses between 0.1 and 3.0 mm from the magnetite-feldspar contact are 1‰ or greater, with one-third (ten analyses) >2‰. Near the contact with garnet (Fig. 2C) a similar but less pronounced pattern is seen where all analyses near the contact are <2‰, and all analyses deeper within the magnetite are >2‰. Analyses between these two areas (Fig. 2A) also average >2‰.

Counting statistics cause a significant uncertainty in the ion microprobe data (±1.0‰). The precision can be improved by averaging multiple analyses from a homogeneous domain; counting statistics improve to ±0.3‰ for ten analyses. In Figure 2A, floating averages show the larger pattern in the entire traverse. The data are subdivided into groups on the basis of the distance from each contact of the magnetite-rich zone. Two groups include the near-contact regions on either side (within 100 $\mu$m of the contact), and the remainder of the data are broken into 1 mm wide blocks. The height of each box in this figure reflects the 1$\sigma$ uncertainty in the mean ($\sigma_\mu$) for each domain, and $\sigma_\mu = \sigma/\sqrt{n}$, where $\sigma$ is the internal precision of a point and $n$ is the number of points.

The profile in Figure 2A has a concave-downward shape that has a relatively steep zone of $\delta^{18}O$ depletion on each

**TABLE 1.** Ion microprobe analyses of magnetite from sample 49-37-14B

| Analysis | $\delta^{18}O_{SMOW}$* | Distance ($\mu$m) | Comments |
|---|---|---|---|
| **24, 25, 26-Jun-92 (drift = 7.2‰, Δ = 11.7‰, standards = ±1.08‰)** | | | |
| LP-204 std | 7.9 | | |
| 14B-2 | 0.6 | 265 | |
| 14B-3 | −0.5 | 870 | |
| 14B-4 | 0.6 | 55 | |
| 14B-5 | 3.9 | | adjacent to biotite |
| LP-204 std | 9.9 | | |
| LP-204 std | 10.0 | | |
| LP-204 std | 7.6 | | |
| 14B-9 | 1.9 | 70 | |
| 14B-10 | 1.5 | 420 | |
| 14B-11 | 0.3 | 560 | |
| 14B-12 | 3.9 | 365 | |
| LP-204 std | 8.5 | | |
| LP-204 std | 7.4 | | |
| LP-204 std | *11.4* | | |
| LP-204 std | 10.2 | | |
| LP-204 std | 8.7 | | |
| 14B-18 | 0.5 | 20 | |
| 14B-19 | 1.1 | 33 | |
| 14B-20 | 3.7 | 980 | |
| 14B-21 | 2.3 | 980 | |
| LP-204 std | 9.5 | | |
| 14B-23 | −1.9 | 25 | |
| 14B-24 | 2.2 | 855 | |
| 14B-25 | 0.7 | 310 | |
| 14B-26 | −1.3 | 25 | |
| 14B-27 | 0.3 | 21 | |
| LP-204 std | 8.2 | | |
| LP-204 std | 8.4 | | |
| 14B-30 | 1.4 | 615 | |
| 14B-31 | *5.1* | 1175 | 2 sd outlier of core values |
| 14B-32 | 3.0 | 1345 | |
| 14B-33 | 3.6 | 1260 | |
| LP-204 std | 10.7 | | |
| 14B-35 | 0.2 | | adjacent to biotite |
| 14B-36 | 2.7 | | adjacent to biotite |
| LP-204 std | 7.9 | | |
| LP-204 std | 9.1 | | |
| 14B-39 | 1.8 | 46 | |
| 14B-40 | −0.3 | 28 | |
| 14B-41 | −0.2 | 35 | |
| LP-204 std | 8.4 | | |
| LP-204 std | 9.9 | | |
| 14B-44 | 1.2 | 98 | |
| 14B-45 | 0.4 | 785 | |
| 14B-46 | 2.8 | 870 | |
| LP-204 std | *7.0* | | |
| LP-204 std | *11.8* | | |
| 14B-49 | 0.3 | 1550 | |
| LP-204 std | 10.4 | | |
| LP-204 std | 9.6 | | |
| LP-204 std | 10.3 | | |
| 14B-53 | 0.9 | 460 | |
| 14B-54 | 2.1 | 2185 | |
| 14B-55 | 0.7 | 2605 | |
| 14B-56 | 2.4 | 2815 | |
| 14B-57 | 0.0 | 812 | |
| LP-204 std | 7.6 | | |
| LP-204 std | 7.0 | | |
| LP-204 std | 8.5 | | |
| **26, 27-Jun-92 (drift = 2.4‰, Δ = 20.1‰, standards = ±0.5‰)** | | | |
| LP-204 std | 8.5 | | |
| LP-204 std | 9.2 | | |
| 14B-63 | 2.2 | *210* | |
| 14B-64 | 1.7 | *70* | |
| 14B-65 | 2.9 | *545* | |
| 14B-66 | 1.1 | *35* | |
| LP-204 std | 8.4 | | |
| 14B-68 | 1.7 | *30* | |
| 14B-69 | 2.1 | *308* | |
| 14B-70 | −1.5 | *28* | |
| LP-204 std | *5.5* | | |
| LP-204 std | 9.7 | | |
| LP-204 std | 9.2 | | |
| 14B-74 | 0.9 | 330 | |
| 14B-75 | 1.8 | 355 | |
| 14B-76 | 1.3 | 1610 | |
| 14B-77 | 1.2 | 1570 | |
| LP-204 std | 8.3 | | |
| 14B-79 | *−3.4* | 730 | 2 sd outlier of core values |
| 14B-80 | 1.6 | 855 | |
| **27-Jul-92 (drift = 4.5‰, Δ = 25.6‰, standards = ±0.3‰)** | | | |
| 14B-81 | 1.6 | 980 | |
| LP-204 std | 8.9 | | |
| LP-204 std | 8.7 | | |
| 14B-84 | 1.0 | 1065 | |
| LP-204 std | 9.2 | | |
| LP-204 std | 8.9 | | |
| 14B-87 | 1.4 | *34* | |
| 14B-88 | 2.5 | *670* | |
| 14B-89 | 1.8 | *38* | |
| 14B-90 | 3.1 | 2740 | *3000* |
| LP-204 std | 8.4 | | |
| LP-204 std | 9.3 | | |

*Note:* LP-204 is a magnetite standard described in Valley and Graham, 1991. Raw data are available on request from J.M.E. Distances to grain boundaries are measured in thin section. Normal type indicates distance to feldspar-magnetite grain boundary, italics indicates distance to magnetite-garnet grain boundary. Both distances are given for 14B-90. The "drift" is the total difference between first and last analysis in a block of data before drift correction. The "Δ" is the average instrumental fractionation, relative to an accepted value for LP 204-1 of +8.9‰. The internal standard deviation (1$\sigma$) is given for the standards of each block (2$\sigma$ outliers are in italics and are not included in the standard deviation).

* Corrected for drift and instrumental mass fractionation (see text).

outer limb. Enlargements of the outermost 800 $\mu$m of each side of the profile (the zones containing the steepest gradients) are shown in Figure 2B and 2C. Also included in these figures are predicted profiles from modeling of volume diffusion between magnetite and feldspar during cooling (discussed below).

## Laser probe analyses

Laser probe analyses were made using a $CO_2$-laser heating and fluorination system (Sharp, 1992; Elsenheimer and Valley, 1993; Kohn et al., 1993). Analyses are standardized against Gore Mountain Garnet (Kohn et al., 1993). The internal precision of laser probe analyses reported in this study is ±0.1‰ (1$\sigma$). All analyses are reported in Table 2.

The 500 $\mu$m thick section used for laser probe analysis is nearly identical to that used for ion microprobe analysis. A partial map of this section can be found in Figure 3. Thirty-eight analyses were made of minerals from three parallel strips cut across the main mineralogical layering. Note that the width of the magnetite layer varies between strips. Feldspar and garnet $\delta^{18}O$ values are nearly homogeneous, within error, averaging 7.9 ± 0.16 and 5.5 ± 0.19‰, respectively. Two analyses of biotite are essentially identical at 5.8 and 6.0‰.

Magnetite, in contrast, is substantially zoned, ranging

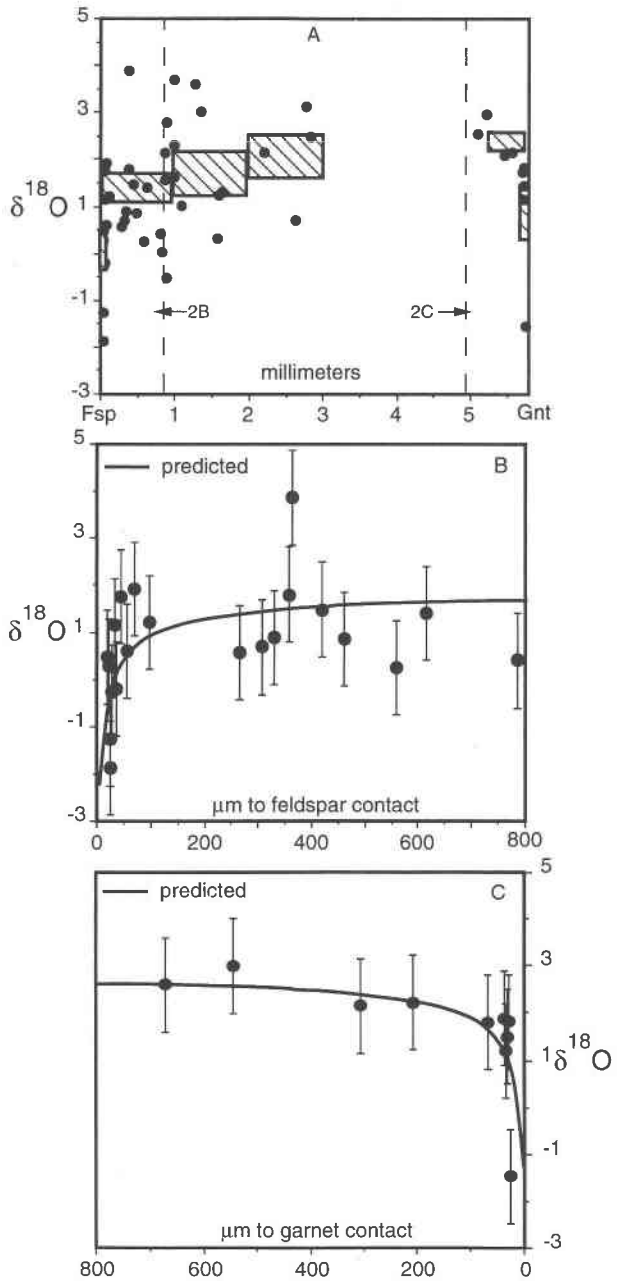


Fig. 2. Ion microprobe analyses of magnetite. (**A**) All data from the feldspar-magnetite contact to magnetite-garnet contact (Fig. 1). Overlays are floating averages. (**B**) Enlarged view of data adjacent to the feldspar-magnetite contact. The predicted profile is based on diffusion modeling and is not fitted to the data. (**C**) Enlarged view of data adjacent to the magnetite-garnet contact. The predicted profile is replotted and set equal to the data furthest from the grain edge in order to illustrate the similarity in shape and magnitude of $\delta^{18}O$ depletion between the two edges of the magnetite layer. Error bars in **B** and **C** are $\pm 1.0‰$ ($1\sigma$).

**TABLE 2.** Laser probe analyses of magnetite, feldspar, garnet, and biotite from sample 49-37-14B, from a section facing the one used for ion microprobe analysis

| Analysis | Mineral | $\delta^{18}O_{Rew}$ | $\delta^{18}O_{SMOW}$ | Distance (mm) |
|---|---|---|---|---|
| **Strip A (23-Jul-93; Gore Mountain Grt = 5.96 ± 0.13)** | | | | |
| 14B-A-1 | Mag | 1.39 | 1.73 | 0–1.0 |
| 14B-A-3 | Fsp | 7.41 | 7.75 | 2.0–3.2 |
| 14B-A-4 | Fsp | 7.30 | 7.64 | 3.2–4.4 |
| 14B-A-5 | Fsp | 7.30 | 7.64 | 4.4–5.6 |
| 14B-A-6 | Fsp | 7.50 | 7.84 | 5.6–6.8 |
| 14B-A-7 | Fsp | 7.79 | 8.13 | 6.8–8.0 |
| 14B-A-8 | Mag | 1.55 | 1.89 | 8.0–9.0 |
| 14B-A-9 | Mag | 2.04 | 2.38 | 9.0–10.0 |
| 14B-A-10 | Mag | 1.87 | 2.21 | 10.0–11.0 |
| 14B-A-11 | Mag | 1.92 | 2.26 | 11.0–12.0 |
| 14B-A-12 | Mag | 1.93 | 2.27 | 12.0–13.0 |
| 14B-A-13 | Grt | 5.20 | 5.54 | 13.0–14.0 |
| 14B-A-16,17,18 | Grt | 5.09 | 5.43 | 16.0–19.0 |
| 14B-A-20 | Grt | 5.54* | 5.88* | 20.0–21.0 |
| **Strip B (16-Oct-93; Gore Mountain Grt = 6.30 ± 0.09)** | | | | |
| 14B-B-1 | Fsp | — | 7.80 | 0–1.6 |
| 14B-B-1,2 | Mag | — | 1.46 | 2.0–4.0 |
| 14B-B-2 | Fsp | — | 7.91 | 1.6–3.2 |
| 14B-B-3 | Fsp | — | 7.80 | 3.2–4.8 |
| 14B-B-4 | Fsp | — | 7.95 | 4.8–6.4 |
| 14B-B-5 | Mag | — | 1.60 | 6.5–8.5 |
| 14B-B-6 | Mag | — | 1.80 | 8.5–10.5 |
| 14B-B-7 | Grt | — | 5.34 | 10.5–11.5 |
| 14B-B-9 | Grt | — | 5.46 | 12.0–13.0 |
| 14B-B-11 | Bt | — | 6.01 | 18.5–20.5 |
| **Strip C (16-Oct-93; Gore Mountain Grt = 6.30 ± 0.09)** | | | | |
| 14B-C-2 | Fsp | — | 8.07 | 1.0–2.2 |
| 14B-C-3 | Fsp | — | 8.02 | 2.2–3.3 |
| 14B-C-4 | Fsp | — | 8.02 | 3.3–4.4 |
| 14B-C-5 | Mag | — | 1.76 | 4.5–5.5 |
| 14B-C-6 | Mag | — | 1.93 | 5.5–6.5 |
| 14B-C-7 | Mag | — | 1.92 | 6.5–7.5 |
| 14B-C-8 | Mag | — | 2.4 | 7.5–8.5 |
| 14B-C-9 | Mag | — | 2.37 | 8.5–9.5 |
| 14B-C-10 | Mag | — | 2.74 | 9.5–10.5 |
| 14B-C-10 | Grt | — | 5.42 | 10.8–12.2 |
| 14B-C-11 | Mag | — | 2.35 | 10.5–11.5 |
| 14B-C-12 | Mag | — | 2.23 | 11.5–12.5 |
| 14B-C-12 | Grt | — | 5.72 | 14.5–15.5 |
| 14B-C-13 | Bt | — | 5.77 | 18.0–20.0 |

*Note:* strips A, B, and C refer to traverses perpendicular to the mineralogical layering in the sample. Fsp = feldspar; Mag = magnetite; Grt = garnet; Bt = biotite.
* Small sample.

from 1.6 to 2.7‰. Values of $\delta^{18}O$ within this range vary systematically with magnetite textures. The strip that most nearly corresponds to the location of the ion microprobe traverse (strip C; Figs. 3 and 4) reveals a concave-downward profile with asymmetry both in the location of the maximum (offset toward the garnet contact) and in the magnitude of the lowest values at the contacts (more depleted near feldspar than near garnet). Comparison of the laser probe profile across strip C with the local averages of the ion microprobe analyses from equivalent spots (Figs. 2A and 4) shows the results to be in agreement, both in shape and absolute value.

Values of $\delta^{18}O$ in the magnetite zone can be contoured, combining self-consistent data from the laser probe and ion microprobe (Fig. 3). Values of $\delta^{18}O$ correlate with the width of the magnetite layer. In strip C the profile contains a maximum at 2.7‰. Where the magnetite zone is 5 mm wide (strip A), magnetite adjacent to the feldspar contact is depleted below 2‰ (as in strip C), but the interior is relatively homogenous at 2.2–2.4‰ (0.3–0.5‰ below the peak in both strip C and the ion microprobe

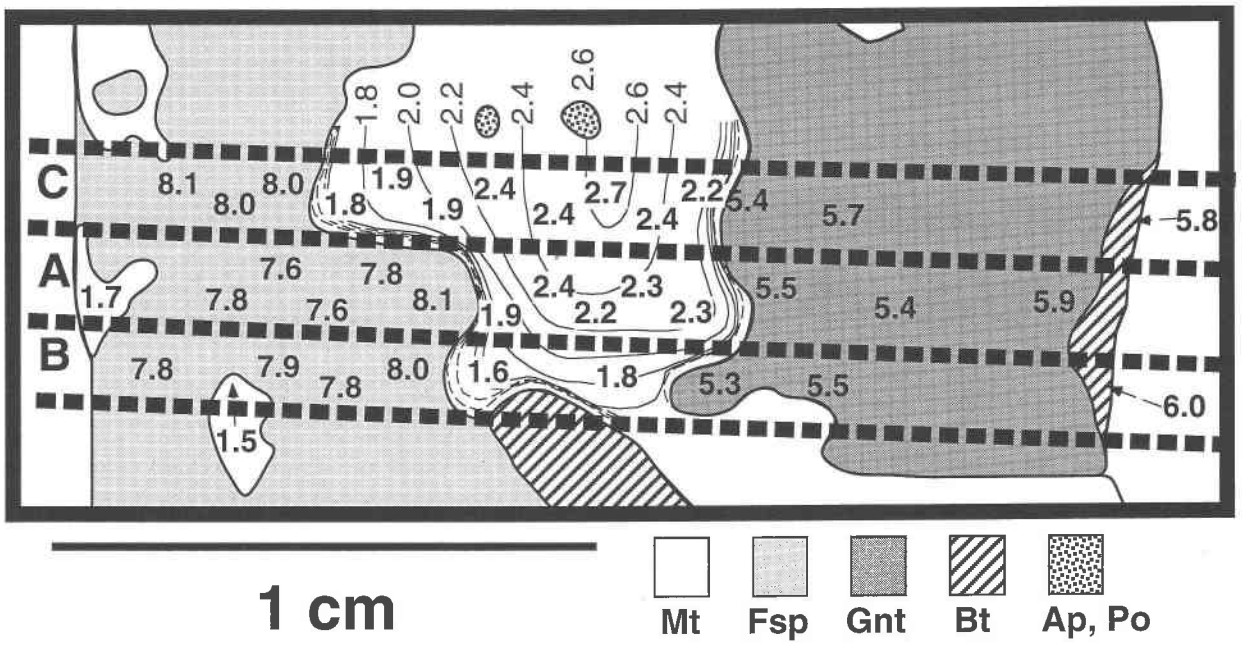


Fig. 3. Laser probe analyses of magnetite and silicates. The thick dashed lines represent saw cuts used to separate strips. Each analysis was of a piece ~1 mm in width. Solid contours (0.2‰) within the magnetite-rich zone are of laser data. Dashed contours (0.5‰) of ion microprobe analyses are shown near each margin, extrapolated onto strips A and B from data obtained in the region corresponding to strip C.

traverse). Where it thins to only 2–4 mm wide (strip B), $\delta^{18}O$ values are below 2‰ throughout (1.6 and 1.8‰). In addition to a 3‰ zonation from core to rim, the magnetite zone therefore has a gradient of 1‰ over 5 mm along its length. The highest $\delta^{18}O$ values are only preserved in the interior of the thickest part of the magnetite zone. Where the seam thins, progressively lower core compositions are preserved. Finally, analyses of disseminated magnetite grains within the feldspar zone show them to have the lowest $\delta^{18}O$, with compositions of 1.5 and 1.7‰.

## Discussion

Several features of the O isotope zonation in magnetite indicate that self-diffusion has reset isotopic compositions during cooling from metamorphic temperatures. As a rock that has equilibrated during metamorphism undergoes uplift and cooling, the equilibrium fractionation of isotopes between its constituent minerals changes (towards larger $^{18}O/^{16}O$ fractionations). In the absence of recrystallization, the degree to which minerals can reequilibrate is limited by the rates of diffusion. The results of diffusion-limited reequilibration include: reset apparent temperatures between minerals, zonation within minerals, and, in special cases where more than two minerals are present in a rock, spuriously high temperatures or even reversed fractionations (Eiler et al., 1992, 1993).

### Intracrystalline zonation

The equilibrium $\delta^{18}O$ of magnetite is the lowest of all the minerals in the sample studied, and so exchange with coexisting phases during cooling will tend to drive its $\delta^{18}O$ value lower still. The relatively slow rate of O diffusion in dry magnetite (Sharp, 1991), as compared with coexisting, high $\delta^{18}O$ feldspar (Giletti et al., 1978; Elphick et al., 1986; Farver and Yund, 1990) produces a diffusion

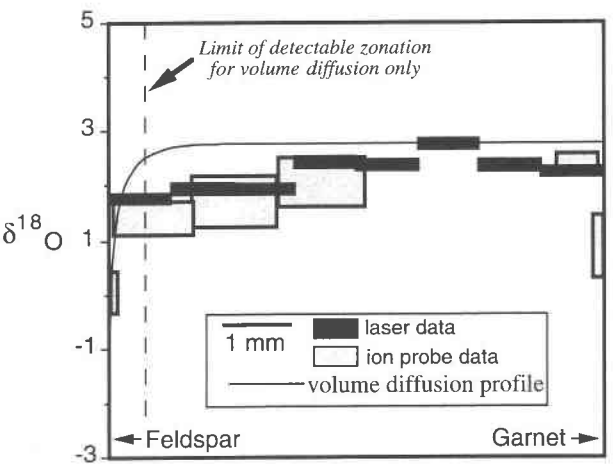


Fig. 4. Laser probe analyses from strip C (dark shading) and local averages of ion microprobe analyses (light shading replotted from Fig. 2A). Solid line is predicted by modeling of volume diffusion for the entire magnetite-rich zone. Low values of $\delta^{18}O$ in magnetite adjacent to garnet indicate that grain boundary diffusion has been significant. The highest $\delta^{18}O$ values in the magnetite are not in the center of the layer but are closer to the garnet contact owing to a combination of volume and grain boundary diffusion.

profile within magnetite. Such profiles are quantitatively predicted by diffusion modeling when, as is the case for this sample, regional cooling rates and mineral diffusion coefficients are known. We have calculated the expected diffusion profile for a magnetite grain undergoing exchange with a touching grain of feldspar using the algorithm described in Eiler et al. (1992). Input for these calculations used a half thickness of 1 mm for both magnetite and feldspar and 50 vol% of each mineral. The actual grain sizes of magnetite and feldspar are 1–2 mm. The actual modal abundances of these minerals are highly variable in this coarsely zoned rock, so a volume abundance of 50% for each was initially chosen to describe interdiffusion only between magnetite and feldspar grains in physical contact with one another, ignoring the contribution from any other grains in the rock. Other models describing exchange across larger portions of this rock will be described below. Calibrations for the volume diffusion coefficients (Sharp, 1991; Giletti et al., 1978) and fractionation factor (Chiba et al., 1989) were taken from the literature. The cooling history was based on known peak temperatures from phase equilibria (Bohlen et al., 1985) and cooling rates from geochronology (Mezger et al., 1990). The calculated profile for magnetite after exchange with touching feldspar is plotted in Figure 2B. The absolute values of $\delta^{18}O$ for the calculated profile are based on the $\delta^{18}O$ of adjacent feldspar and are independent of the ion microprobe data.

The predicted profile passes through the $1\sigma$ bracket of most of the ion microprobe analyses at the feldspar-magnetite contact (Fig. 2B). Because uncertainties in individual ion microprobe measurements are relatively large, a more rigorous comparison between model and data is found by comparing averages of two populations of data (near-rim and core analyses) with the calculated profile. The analyses collected within 100 $\mu$m of the contact average $\delta^{18}O = 0.1 \pm 1.1$‰, with an uncertainty in the mean ($\sigma_\mu$) of $\pm 0.4$‰. In contrast, the average of all analyses more than 100 $\mu$m from the contact (on the feldspar side of the magnetite zone) is $1.6 \pm 1.2$‰ ($\sigma_\mu = \pm 0.2$‰), yielding a minimum core-rim zonation of $1.5 \pm 0.4$‰. A better estimate of core composition would use only laser data and ion probe analyses >1 mm from the contact (2.0–2.3‰). This yields a difference of 1.9–2.2‰. The difference between these two regions is predicted to be 1.9‰, as shown by the solid line in Figure 2B. Zonation seen in the ion microprobe data within 1 mm of the feldspar-magnetite contact is therefore consistent with control of retrogression by local diffusional exchange.

The exceptionally slow rate of O self-diffusion in garnet prohibits it from being a reservoir for interdiffusion in this rock (Coghlan, 1990). However, when the predicted profile for magnetite-feldspar exchange is plotted with the data for the magnetite-garnet contact (Fig. 2C) the similarity is striking. The analyses of grain cores on this side of the magnetite seam average $2.4 \pm 0.3$‰ ($\sigma_\mu = \pm 0.16$‰), whereas the analyses of grain rims average $0.9 \pm 1.3$‰ ($\sigma_\mu = \pm 0.6$‰). The difference ($1.5 \pm 0.6$‰) is in the same direction and magnitude to the predicted difference from volume-diffusion modeling of exchange between feldspar and magnetite. The similarity in direction and magnitude of this zonation to both that predicted by diffusion modeling and that observed where magnetite touches feldspar suggests that magnetite zonation adjacent to garnet is the product of a similar process. We propose that zonation adjacent to garnet was produced by diffusional exchange with nontouching grains of silicate, most likely feldspar, making use of grain boundaries as intermediate pathways for exchange. The millimeter-scale zonation present in this sample provides supporting evidence for this explanation.

### Intercrystalline zonation

Three features can be distinguished in the millimeter-scale zonation (Fig. 3): (1) a core-to-rim decrease in $\delta^{18}O$ of the magnetite zone, more gentle than, but continuous with the steeper zonation adjacent to the outer edges of the magnetite zone; (2) a decrease in the $\delta^{18}O$ of the interior of the magnetite seam as it thins; and (3) asymmetry in the core-to-rim zonation of the magnetite zone, such that $\delta^{18}O$ values are lower at the feldspar contact than at the garnet contact. All these features are inconsistent with volume diffusion acting alone but are expected if diffusion has been short-circuited by grain boundaries.

Figure 4 shows the laser probe analyses from traverse C along with floating averages from the ion microprobe traverse (Fig. 2A) and a profile predicted to form across the entire magnetite zone during cooling, calculated assuming grain boundaries have not contributed to diffusion (a half-width of 7 mm is used for magnetite to model the entire layer, ignoring magnetite-magnetite grain boundaries). With the use of the methods and constraints described above for the calculations presented in Figure 2, two calculations were made (one for magnetite-feldspar exchange, the other for magnetite-garnet exchange) and the two profiles superimposed. This calculation describes interdiffusion during cooling only between touching mineral grains.

The calculations indicate that volume diffusion acting alone is incapable of producing zonation more than 500 $\mu$m from the feldspar contact, and that, under these conditions, no zonation at any scale should be produced at the contact between magnetite and garnet. The data deviate from the curve toward both contacts, demonstrating that some process facilitated exchange between magnetite and feldspar 4–5 mm deeper into the magnetite-rich zone than volume diffusion would allow and permitted magnetite at the garnet contact to exchange O isotopes with a reservoir beyond the adjacent garnet.

Grain boundaries and intergranular fluids are known to produce zones of relatively rapid diffusion in rocks, having rates 6–8 orders of magnitude faster than volume diffusion in magnetite (Brady, 1983; Nagy and Giletti, 1986; Joesten and Fisher, 1988; Joesten, 1991; Farver and Yund, 1991). Even for the low porosities probably present in an anhydrous, annealed, granulite facies rock, these enhanced rates can serve to explain the millimeter-

scale zonation observed. This effect is most readily expressed in the Hart equation for the calculation of bulk diffusion coefficients in polygranular media (Hart, 1957):

$$D_{bulk} = \tau[(1 - \alpha)D_{vol} + \alpha D_{gb}]$$

where $D_{bulk}$ is the effective diffusion coefficient of a polycrystalline matrix, $D_{vol}$ is the volume diffusion coefficient of the constituent minerals, $D_{gb}$ is the diffusion coefficient of the grain boundary medium, $\tau$ is the tortuosity of the grain boundary network (typically ~0.5: Brady, 1983), and $\alpha$ is the volume fraction of the grain boundary network. The Hart equation was devised to describe the effect of enhanced diffusion on planar defects within mineral grains but is equally well suited to describing the effect of enhanced diffusion along grain boundaries or through grain boundary fluids on the bulk diffusion coefficient. The simple form of the Hart equation is the result of an assumption that the volume diffusion distance over the time of interest $[(D_{vol}t)^{1/2}]$ is relatively large, on the order of a grain width or larger (Harrison, 1961). This condition is just met in the case of magnetite undergoing the integrated cooling history for the Adirondack Mountains.

Given porosities ($\alpha$) of $10^{-6}$ [corresponding to grain boundary widths, $x$, of 1 nm through the relationship $\alpha = (\pi x)/(2d)$, where $d$ is the grain diameter], the Hart equation indicates that experimental grain boundary diffusion rates (Nagy and Giletti, 1986; Farver and Yund, 1991) are fast enough to enhance bulk diffusion distances in polygranular magnetite by approximately a factor of ten over the volume diffusion coefficient for individual magnetite grains. This leads to an increase of the integrated diffusion distance in bulk magnetite from several hundred micrometers for volume diffusion alone (Figs. 2A and 4) to several millimeters for polygranular magnetite with rapid diffusion through the grain boundary region. This amount of enhancement can explain the extension of depleted $\delta^{18}O$ values 5 mm within the magnetite zone (Fig. 4). The asymmetry to the profile found in the laser data and suggested in the ion microprobe data (i.e., the lesser degree of exchange where magnetite touches garnet) is consistent with these features because one expects exchange through an intervening grain boundary to be at least partially restricted relative to exchange between touching grains.

## Conclusions

The results presented in this study document the complex zonation produced on both the millimeter- and micrometer-scales by diffusive exchange of stable isotopes during cooling. Micrometer-scale zonation within individual grains is controlled by volume diffusion, while that at the millimeter-scale is dependent upon both diffusion through the grain boundary region and volume diffusion. There is a strong interaction between these two pathways, such that isotope diffusion in a rock is best thought of as a process with contributions from both of two interpenetrating media: the grains and the grain boundaries or intergranular fluids (Fisher, 1951; Hart, 1957; LeClaire, 1963; Wang, 1993).

This result has several implications for the routine application of stable isotope geochemistry to high-temperature, slowly cooled rocks. Isotopic compositions may be strongly texturally dependent. In the sample studied this effect has led to the best preserved (i.e., highest) $\delta^{18}O$ value in magnetite not being in the geometric center of the magnetite zone. In a routine application of stable isotope thermometry, the location of the best preserved composition is a first-order question, and even the cautious researcher who analyzes only the cores of mineral zones would in this case be mistaken: the geometric core of the zone has been reset by 0.5‰, and the peak composition is preserved closer to one of the grain boundaries. Sampling too close to that seemingly inert contact between magnetite and garnet, however, would yield an even more reset composition. This result provides graphic evidence that our analysis of isotopic compositions in such settings must be guided by an appreciation of the complex network of pathways by which isotopes are redistributed in rocks.

Many observations seen in this study were due to the sample being mineralogically zoned on the scale of a centimeter. Transport through grain boundaries has facilitated exchange enough to have a considerable effect on diffusion distances but not enough to overcome the coarse mineralogical zonation. These complexities are avoided in a rock in which grain sizes and textural zonation are equal to or smaller than the bulk diffusion distances. The assumption of homogeneous grain boundary compositions used in the fast grain boundary diffusion model (Eiler et al., 1992, 1993) should be met in high-grade regional metamorphic rocks with a homogeneous texture and grain sizes on the order of 1 mm or smaller. In addition to knowing grain sizes and modal abundances, one must consider the characteristic scale of textural homogeneity before determining the effects of diffusion during cooling or undertaking routine stable isotope thermometry on mineral separates.

## Acknowledgments

We wish to acknowledge the financial support of the National Science Foundation, the Department of Energy, the Wisconsin Alumni Research Foundation, the Geological Society of America, and Sigma Xi. Thorough and helpful reviews by Ray Joesten and Jean Morrison substantially improved this paper. We also thank Stuart Kearns of the University of Edinburgh for his assistance with electron microprobe analysis, Rick Noll at the University of Wisconsin for his assistance with the SEM, Eugene Cameron for providing the sample used in this study, and Mike Spicuzza and Matt Kohn for help and training in laser probe analysis. Particular thanks are due as well to John Craven for assistance, training, and advice in the use of the Edinburgh ion microprobe, which is supported by NERC.

## References cited

Bohlen, S.R., Valley, J.W., and Essene, E.J. (1985) Metamorphism in the Adirondacks: I. Petrology, pressure and temperature. Journal of Petrology, 26, 971–992.

Brady, J.B. (1983) Intergranular diffusion in metamorphic rocks. American Journal of Science, 283A, 181–200.

——— (1995) Diffusion data for silicate minerals, glasses and liquids. In T.H. Ahrens, Ed., AGU handbook of physical constants, in press.

Chiba, H., Chacko, T., Clayton, R.N., and Goldsmith, J.R. (1989) Oxygen isotope fractionations involving diopside, forsterite, magnetite and cal-

cite: Applications to geothermometry. Geochimica et Cosmochimica Acta, 53, 2985–2995.

Coghlan, R.A. (1990) Studies in diffusional transport: Grain boundary transport of O in feldspars, diffusion of O, Sr and the REE's in garnet, and thermal histories of granitic intrusions in south-central Maine using O isotopes. Ph.D. thesis. Brown University, Providence, Rhode Island.

Eiler, J.M., Baumgartner, L.P., and Valley, J.W. (1992) Interdiffusion of stable isotopes: A fast grain boundary model. Contributions to Mineralogy and Petrology, 112, 543–557.

Eiler, J.M., Valley, J.W., and Baumgartner, L.P. (1993) A new look at stable isotope thermometry. Geochimica et Cosmochimica Acta, 57, 2571–2583.

Eiler, J.M., Valley, J.W., Graham, C.M., and Baumgartner, L.P. (1995) Ion microprobe evidence for the mechanisms of stable isotope retrogression in high-grade metamorphic rocks. Contributions to Mineralogy and Petrology, 118, 365–378.

Elphick, S.C., Dennis, P.F., and Graham, C.M. (1986) An experimental study of the diffusion of oxygen in quartz and albite using an overgrowth technique. Contributions to Mineralogy and Petrology, 92, 322–330.

Elsenheimer, D., and Valley, J.W. (1993) Submillimeter scale zonation of $\delta^{18}O$ in quartz and feldspar, Isle of Skye, Scotland. Geochimica et Cosmochimica Acta, 57, 3669–3676.

Farver, J.R., and Yund, R.A. (1990) The effect of hydrogen, oxygen, and water fugacity on oxygen diffusion in alkali feldspar. Geochimica et Cosmochimica Acta, 54, 2953–2964.

——— (1991) Measurement of oxygen grain boundary diffusion in natural, fine-grained quartz aggregates. Geochimica et Cosmochimica Acta, 55, 1597–1608.

Fisher, J.C. (1951) Calculation of diffusion penetration curves for surface and grain boundary diffusion. Journal of Applied Physics, 22, 74–77.

Freer, R. (1981) Diffusion in silicate minerals and glasses: A data digest and guide to the literature. Contributions to Mineralogy and Petrology, 76, 440–454.

Giletti, B.J., Semet, M.P., and Yund, R.A. (1978) Studies in diffusion: III. Oxygen in feldspars, an ion microprobe determination. Geochimica et Cosmochimica Acta, 42, 45–57.

Harrison, L.G. (1961) Influence of dislocations on diffusion kinetics in solids with particular reference to alkali halides. Transactions of the Faraday Society, 57, 1191–1199.

Hart, E.W. (1957) On the role of dislocations in bulk diffusion. Acta Metallica, 5, 597.

Hervig, R.L. (1992) Oxygen isotope analysis using extreme energy filtering. Chemical Geology, 101, 185–186.

Joesten, R. (1991) Grain boundary diffusion kinetics in silicate and oxide minerals. In Advances in Physical Geochemistry, 8, 345–395.

Joesten, R., and Fisher, G.W. (1988) Kinetics of diffusion controlled mineral growth in the Christmas Mountains (Texas) contact aureole. Geologic Society of America Bulletin, 100, 714–732.

Kohn, M.J., Valley, J.W., Elsenheimer, D., and Spicuzza, M.J. (1993) O isotope zoning in garnet and staurolite: Evidence for closed-system mineral growth during regional metamorphism. American Mineralogist, 78, 988–1001.

Lasaga, A.C. (1983) Geospeedometry: An extension of geothermometry. In Kinetics and equilibrium in mineral reactions, vol. 3: Advances in physical chemistry, p. 81–114. Springer-Verlag, New York.

LeClaire, A.D. (1963) The analysis of grain boundary diffusion measurements. British Journal of Applied Physics, 14, 351–356.

Marcotty, L.A. (1985) The petrology of the magnetite paragneisses at Benson Mines, Adirondacks, New York. M.S. thesis, University of Michigan, Ann Arbor, Michigan.

McLelland, J.M., and Chiarenzelli, J. (1991) Geochronological studies in the Adirondack Mountains and the implications of a middle Proterozoic tonalite suite. In Mid-Proterozoic geology of the southern margin of Laurentia-Baltica, Geologic Association of Canada Special Paper 38, 175–194.

McLelland, J.M., Chiarenzelli, J., Whitney, P., and Isachsen, Y. (1988) U-Pb zircon geochronology of the Adirondack Mts. and implications for their tectonic evolution. Geology, 16, 920–924.

Mezger, K., Rawnsley, C., Bohlen, S.R., and Hanson, G.N. (1990) U-Pb garnet, sphene, monazite, and rutile ages: Implications for the duration of high-grade metamorphism and cooling histories, Adirondack Mts., New York. Journal of Geology, 99, 415–428.

Nagy, K.L., and Giletti, B.J. (1986) Grain boundary diffusion of oxygen in macroperthitic feldspar. Geochimica et Cosmochimica Acta, 50, 1151–1158.

Sharp, Z.D. (1991) Determination of oxygen diffusion rates in magnetite from natural isotopic variations. Geology, 19, 653–656.

——— (1992) In situ laser microprobe techniques for stable isotope analysis. Chemical Geology, 101, 3–19.

Valley, J.W., and Graham, C.M. (1991) Ion microprobe analysis of oxygen isotope ratios in granulite facies magnetites: Diffusive exchange as a guide to cooling history. Contributions to Mineralogy and Petrology, 109, 38–52.

——— (1993) Cryptic grain-scale heterogeneity of oxygen isotope ratios in metamorphic magnetite. Science, 259, 1729–1733.

Wang, H.F. (1993) Double medium diffusion in rocks with a small, continuous fluid phase. Contributions to Mineralogy and Petrology, 114, 357–364.

MANUSCRIPT RECEIVED SEPTEMBER 2, 1994
MANUSCRIPT ACCEPTED MARCH 13, 1995